

*Invited paper***A novel-high energy pulse compression system: generation of multigigawatt sub-5-fs pulses**M. Nisoli¹, S. Stagira¹, S. De Silvestri¹, O. Svelto¹, S. Sartania², Z. Cheng², M. Lenzner², Ch. Spielmann², F. Krausz²¹Centro di Elettronica Quantistica e Strumentazione Elettronica - CNR, Dipartimento di Fisica, Politecnico, Piazza L. da Vinci 32, 20133 Milano, Italy²Abteilung Quantenelektronik und Lasertechnik Technische Universität Wien, Gusshausstr. 27, A-1040 Wien, Austria

Received: 28 February 1997 / Revised version: 2 May 1997

Abstract. Powerful techniques for spectral broadening and ultrabroadband dispersion control, which allow the compression of high-energy femtosecond pulses to a duration of a few optical cycles, are presented. Spectral broadening by propagation along hollow-core fused silica fiber filled with atomic and molecular gases is studied under two excitation regimes with high-energy input pulses of 140 fs and 20 fs duration respectively. Conditions for optimum pulse compression are outlined considering the role of self-phase modulation and gas dispersion in the two regimes. With 20 fs input pulses and under optimum compression conditions we demonstrate a pulse shortening down to 4.5 fs with output energy up to 70 μ J using a high-throughput prism-chirped-mirror delay line. These pulses are the shortest generated to date at multigigawatt peak power.

PACS: 42.65.Re; 42.65.Vh

Ultrashort-pulse lasers are the most important experimental tools for investigating fast-evolving atomic and molecular dynamics in physics, chemistry, and biology. In the last few years, great technological advances have been made in the field of ultrafast pulse generation. New mode-locking techniques such as additive-pulse mode-locking and Kerr-lens mode-locking have been successfully used for femtosecond pulse generation from a wide range of solid-state laser oscillators [1]. Using chirped mirrors [2] for intracavity dispersion control, pulses down to 7.5 fs have been directly generated by a Kerr-lens mode-locked Ti:sapphire oscillator [3] and, more recently, 6.5-fs pulses have been obtained using broadband semiconductor saturable absorbers for self-starting [4]. Ti:sapphire amplifiers seeded by femtosecond laser oscillators can now generate pulses of 20–30 fs with gigawatt [5, 6] or terawatt [7–9] peak power at repetition rates in the kHz and 10 Hz regimes, respectively. Ultrashort pulses can also be generated by extracavity compression techniques, in which the pulses are spectrally broadened upon propagation in a suitable nonlinear waveguide and subsequently compressed in a carefully designed optical dispersive delay line. Spectral broadening of laser pulses by self-phase modulation

(SPM) in a single-mode optical fiber is a well-established technique: pulses down to 6 fs were obtained in 1987 from 50-fs pulses from a mode-locked dye laser [10]. More recently 13-fs pulses from a cavity-dumped Ti:sapphire laser were compressed to 5 fs with the same technique [11]. However, the use of single-mode fibers limits the pulse energy to a few nanojoules. A powerful pulse compression technique based on spectral broadening in an hollow fiber filled with noble gases has demonstrated the capability of handling high-energy pulses (sub-mJ range) [12]. This technique presents the advantages of a guiding element with a large diameter mode and of a fast nonlinear medium with high threshold for multiphoton ionization. New concepts in the construction of dispersive delay lines have been applied in the development of specially designed chirped mirrors for fine control of cubic and quartic phase dispersion terms over a large spectral bandwidth [3]. The implementation of the hollow-fiber technique using 20-fs seed pulses from a Ti:sapphire system [5] and a high-throughput broadband dispersive delay line consisting of prisms and chirped mirrors has recently permitted the generation of multigigawatt sub-5 fs pulses [13].

In this paper we present a comprehensive analysis of compression experiments with high-energy femtosecond pulses performed using gas-filled hollow fibers. Spectral broadenings obtained in different gases are compared for 140-fs and 20-fs input pulses generated by Ti:sapphire laser systems, and the optimum conditions for pulse compression are outlined considering the role of SPM and gas dispersion. A new ultrabroadband prism-chirped-mirror dispersive delay line, characterized by a high throughput and dispersion control up to the fourth order, is described in detail. The paper is organized as follows. In Sect. 1 we provide a description of hollow fiber modes and discuss the major advantages of this device compared to optical fibers. Sect. 2 reports on typical spectral broadenings achieved under different excitation conditions. In Sect. 3 we report on the characteristics of the prism-chirped-mirror compressor and discuss the experimental results obtained with 20-fs input pulses. Under optimum compression conditions we show a pulse shortening down to 4.5 fs with output energy up to 70 μ J. These pulses are the

shortest generated to date at multigigawatt peak power. In Sect. 4 the characteristics of the output beam after compression are reported. Finally, the new prospects in high-field light matter interactions opened up by the results reported in this work are discussed in Sect. 5.

1 Propagation modes and losses in hollow fibers

The use of hollow fibers allows the exploitation of a spatially uniform SPM and overcomes the limitation imposed on the pulse energy by the small core diameters of single-mode fibers. Owing to the large and scalable mode size, this technique can handle much higher pulse energies than traditionally used single-mode optical fibers.

Wave propagation along hollow guides can be thought of as occurring by grazing incidence reflections at the dielectric inner surface. Since the losses caused by these multiple reflections greatly discriminate against higher-order modes, only the fundamental mode will be transmitted through a sufficiently long fiber. This offers the potential for using a large channel diameter without compromising the quality of the output beam. The modes of hollow cylindrical fibers with diameters much larger than the wavelength were considered by Marcatili and Schmeltzer [14]. These fibers support three types of modes: transverse circular electric (TE_{0m}), in which the electric field lines are transverse concentric circles centered on the propagation axis, transverse circular magnetic (TM_{0m}), with the electric field directed radially, and hybrid modes EH_{pm} ($|p| \geq 1$), with all the electric and magnetic components present (the axial field components are relatively small so that the hybrid modes are almost transverse). The mode with lowest attenuation is TE_{01} if the refractive index of the external medium is greater than 2.02 times that of the internal medium, in the other cases the fundamental mode is EH_{11} . For fused silica gas-filled hollow fibers the lowest-loss mode is the EH_{11} hybrid mode, whose intensity profile as a function of the radial coordinate r is given by:

$$I(r) = I_0 J_0^2(2.405r/a) \quad (1)$$

where I_0 is the peak intensity, J_0 is the zero-order Bessel function and a is the capillary radius. For the same mode the real, β (phase constant), and imaginary, $\alpha/2$ (field attenuation constant), parts of the propagation constant are given by [14]:

$$\beta = \frac{2\pi}{\lambda} \left[1 - \frac{1}{2} \left(\frac{2.405\lambda}{2\pi a} \right)^2 \right], \quad (2)$$

$$\frac{\alpha}{2} = \left(\frac{2.405}{2\pi} \right)^2 \frac{\lambda^2}{2a^3} \frac{\nu^2 + 1}{\sqrt{\nu^2 - 1}}, \quad (3)$$

where λ is the laser wavelength in the gas medium and ν is the ratio between the refractive indices of the external (fused silica) and internal (gas) media. Since the attenuation constant is proportional to λ^2/a^3 , the losses can be made arbitrarily small by choosing a capillary radius sufficiently large relative to the wavelength λ . This is shown in Fig. 1a in which we have plotted the transmission of the fundamental EH_{11} mode at a wavelength of 780 nm as a function of the hollow fiber length for different values of the capillary radius a , ranging from 30 μm to 90 μm . An important issue to be considered

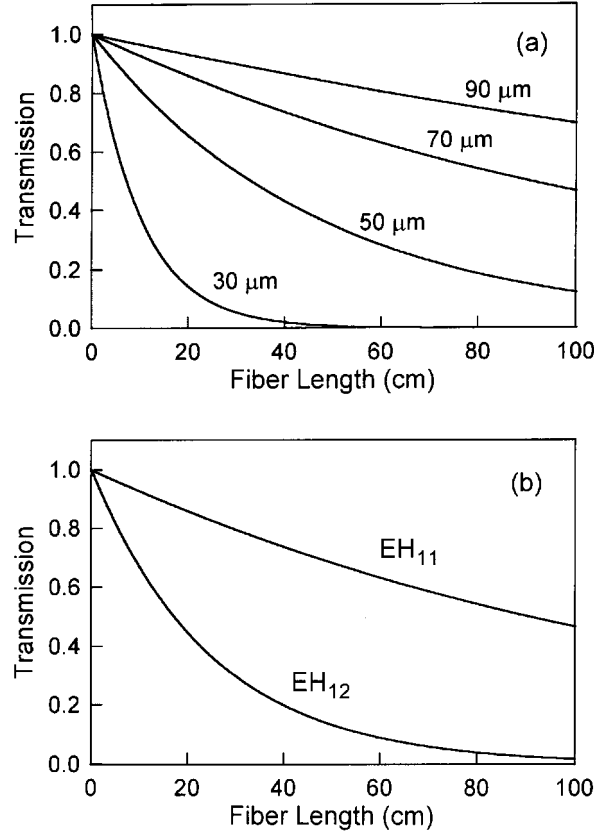


Fig. 1. **a** Transmission of the fundamental mode (EH_{11}) at 780 nm as a function of hollow fiber length for different values of the capillary radius **b** Transmission of the EH_{11} mode and next high-order mode EH_{12} for a 70 μm capillary radius as a function of fiber length

is the discrimination of the fundamental mode from higher order-modes. Figure 1b shows the calculated transmission of the EH_{11} fundamental mode and that of the subsequent, linearly polarised, hybrid mode EH_{12} for a hollow fiber with a capillary radius of 70 μm , at 780 nm, as a function of the fiber length. As is evident from the figure, for sufficiently long fibers the mode discrimination is very high so that only the fundamental mode can propagate. The transverse mode purity of the beam exiting the waveguide can be significantly better than that suggested by Fig. 1b for large capillary radii, provided that the incident radiation is dominantly coupled into the fundamental propagation mode by proper mode matching.

2 Spectral broadening by hollow fibers

2.1 Experimental set-up

The experiments reported in this and the following sections were performed using two different excitation sources. A first series of experiments was carried out by using a Ti:sapphire laser with chirped-pulse amplification (CPA-1 by Clark-MXR), which provides 140-fs pulses at 780 nm, with energy up to 660 μJ at a 1-kHz repetition rate. A second series of experiments was carried out by using a Kerr-lens mode-locked mirror-dispersion-controlled Ti:sapphire oscillator, which provides nearly transform-limited 8-fs pulses. These pulses

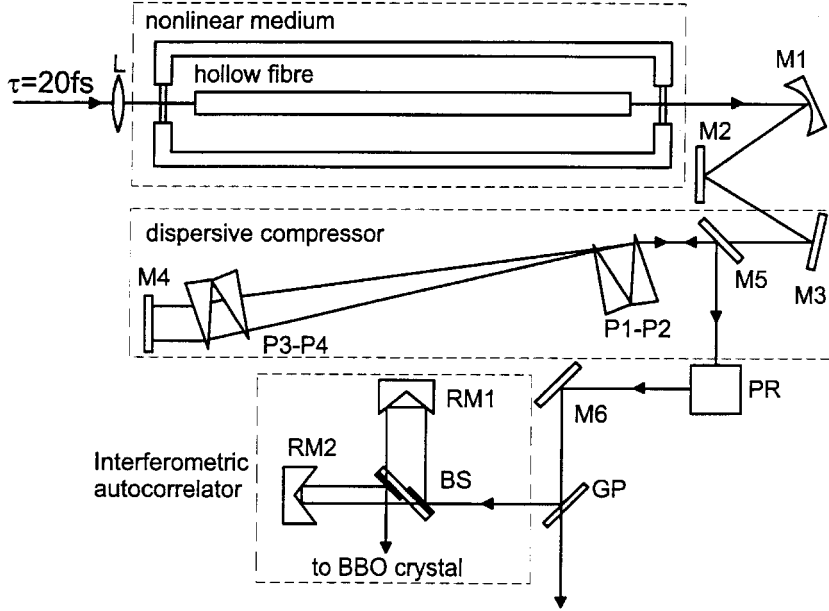


Fig. 2. Schematic diagram of the experimental setup. L is an AR-coated lens of 30 cm focal length, $M1$ is a silver-coated mirror with 50 cm radius of curvature; $M2$, $M5$, and $M6$ are silver-coated plane mirrors and $M3$, $M4$ are chirped multilayer mirrors; $P1$ – $P4$ are AR-coated multilayer 20° fused silica prisms (the prismatic delay line is folded by a silver-coated mirror not shown in the figure). The beam reflected back by $M4$ is slightly separated from the incident beam to allow coupling by $M6$. PR provides polarization rotation using silver-coated mirrors. GP is a 1-mm-thick fused silica plate with AR-coated back side. BS is a broadband dielectric beam splitter on a fused silica substrate identical to GP . $RM1$ and $RM2$ are silver-coated roof mirror assemblies

were amplified at a repetition rate of 1 kHz in a multipass amplifier pumped by the second harmonic of a Q-switched Nd:YLF laser [5]. The output pulses have a duration of 20 fs, energy up to 300 μ J and a spectrum centered on 780 nm. Both amplifier systems delivered approximately transform-limited pulses. Fused silica hollow fibers of 60–70 cm length and 70–80 μ m capillary radius were used. The fiber was kept straight in a V-groove made in an aluminium bar, which was then placed in a pressurized chamber. The laser beam entered the chamber through 1-mm thick fused silica windows coated for broadband antireflection (see Fig. 2). The chamber was filled with several gases such as argon, krypton, and nitrogen at different pressures. The overall throughput of the pressurized chamber, including coupling and fiber losses as well as some residual reflection losses at the antireflection-coated windows, was ≈ 50 –65%, for the various fibers used in the experiments, close to the values predicted by (3). This indicates that bending and surface-roughness losses are negligible in our case.

2.2 Spectral broadening with atomic and molecular gases

Pulse propagation in a hollow fiber filled with gases can be described by the same equations used for the case of optical fibers. The relative weights of SPM and dispersion can be evaluated using characteristic parameters such as the nonlinear length L_{nl} and the dispersion length L_d , defined as [15]: $L_{nl} = 1/(\gamma P_0)$ and $L_d = T_0^2/|\beta_2|$, where $\beta_2 = d^2\beta/d\omega^2$ is the group velocity dispersion (GVD) of the fiber filled with gas, P_0 is the peak power of the pulse and T_0 is the half-width (at the 1/e-intensity point) of the pulse. The nonlinear coefficient γ is given by $\gamma = n_2\omega_0/cA_{eff}$, where ω_0 is the center laser frequency, c is the light speed in vacuum, n_2 is the nonlinear index coefficient ($n = n_0 + n_2I$, where I is the field intensity) and A_{eff} is the effective mode area. Optimum exploitation of the interplay between GVD and SPM for the generation of linearly chirped pulses calls for a propagation length $L_{opt} \approx (6L_{nl}L_d)^{1/2}$ [16]. In what follows, SPM-induced spectral broadening in a hollow fiber filled with noble

gases such as argon and krypton will be reported both for 140-fs and 20-fs input pulses. An example of spectral broadening achieved using a molecular gas such as nitrogen is also reported under the above excitation conditions.

2.2.1 Argon. Figure 3a shows the output spectrum measured by using 140-fs input pulses at peak power $P_0 = 3.5$ GW for a gas pressure $p = 4$ bar. The spectrum shows amplitude modulations that are characteristic of a pure SPM process. Assuming for argon $n_2/p = 9.8 \times 10^{-24}$ m²/Wbar [17], one obtains $L_{nl} \approx 0.66$ cm for a capillary radius of 70 μ m. On considering the contributions to second-order dispersion from both gas [18] and fiber [14], one gets a value of $\beta_2 \approx 48$ fs²/m which gives $L_d \approx 131$ m. These values give $L_{opt} \approx 2.3$ m, which turns out to be much longer than the fiber length (70 cm). Therefore, the effect of dispersion is almost negligible, as observed experimentally. The observed linear dependence of the spectral broadening on gas pressure suggests that nonlinear refractive index contributions arising from atom-atom interactions are negligible at these pressures. With 20-fs input pulses, the spectral broadening presents a different behavior. A typical shape of the spectrum measured at the output of the fiber for an argon pressure $p = 3.3$ bar and an input peak power $P_0 = 4$ GW is shown in Fig. 3b. The shape of the spectrum is much more uniform than that obtained with 140-fs input pulses. This indicates that, at this shorter pulse duration, gas dispersion, in addition to SPM, also plays an important role during pulse propagation. In fact, in this case one obtains $L_{nl} \approx 0.92$ cm (for a capillary radius of 80 μ m) and $L_d \approx 3.2$ m ($\beta_2 \approx 40$ fs²/m), so that the optimum length turns out to be $L_{opt} \approx 42$ cm, which is somewhat shorter than that used in the experiments. However, if one takes into account the peak power reduction during propagation, which tends to increase L_{nl} , the length of the fiber is not too far from optimum. As is evident from Fig. 3, 20-fs pulses produce a much larger spectral broadening than 140-fs pulses in the experimental conditions described above. To understand the physical processes that lead

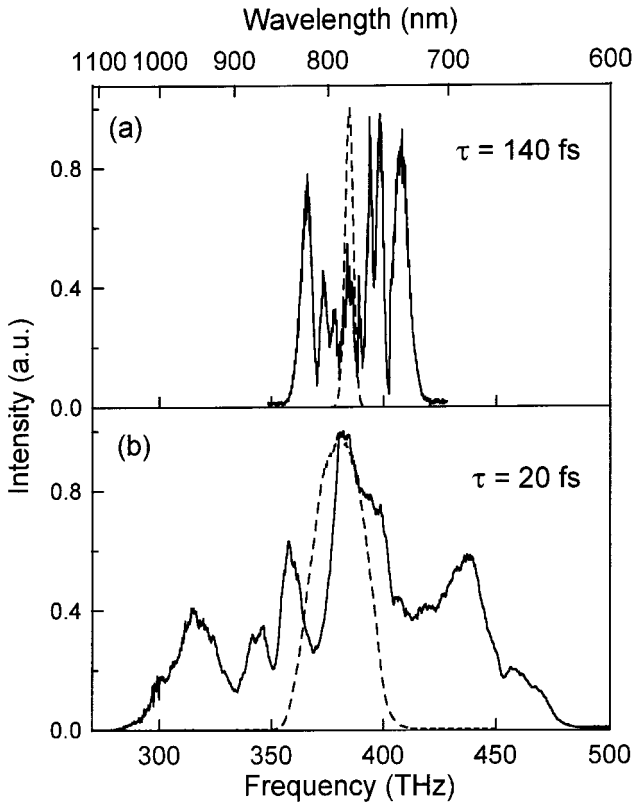


Fig. 3. Spectral broadening in argon (a) at $p = 4$ bar and $P_0 = 3.5$ GW obtained with 140-fs input pulses; (b) at $p = 3.3$ bar and $P_0 = 4$ GW obtained with 20-fs input pulses. A low-intensity pedestal (approximately 1% of the peak) on the short wavelength side extends somewhat below 600 nm. The spectra of the input pulses are shown as *dashed lines*

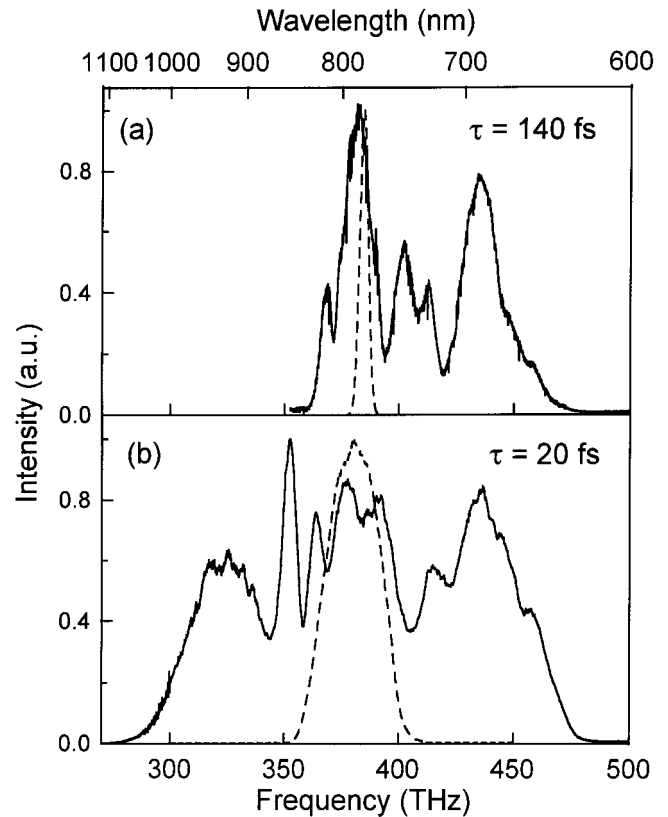


Fig. 4a,b. Spectral broadening in krypton (a) at $p = 2$ bar for $P_0 = 3.5$ GW obtained with 140-fs input pulses, and (b) at $p = 2.1$ bar and $P_0 = 2$ GW obtained with 20-fs input pulses. A low-intensity pedestal (approximately 1% of the peak) on the short wavelength side extends somewhat below 600 nm. The spectra of the input pulses are shown as *dashed lines*

to the observed behavior, we have performed computer simulations of the pulse propagation along the hollow fiber taking into account the self-steepening effect and the dispersion up to the third order. The calculated spectral broadening, in the above experimental conditions, turns out to be ~ 2.4 times larger in the case of 20-fs pulses than in the case of 140-fs pulses, in good agreement with the results shown in Fig. 3.

2.2.2 Krypton. A typical broadened spectrum measured at $p = 2$ bar of krypton and $P_0 = 3.5$ GW in the case of 140 fs input pulses is shown in Fig. 4a. The shape is somewhat asymmetric and more uniform compared to that observed with argon. The greater extension to the blue side of the input laser wavelength is a consequence of self-steepening, which has previously been observed in liquids, solids [19, 20] and optical fibers [21]. In fact, by decreasing P_0 to 1 GW the spectrum becomes symmetric. The steeper trailing edge of the pulse implies larger spectral broadening on the blue side since SPM generates blue components near the trailing edge. According to our experimental conditions, the critical distance corresponding to shock formation [15], in the absence of dispersion, turns out to be of the order of the fiber length (70 cm). Assuming for krypton $n_2/p = 2.78 \times 10^{-23} \text{ m}^2/\text{Wbar}$ [17], one obtains $L_{\text{nl}} \approx 0.47$ cm for a capillary radius of 70 μm . On considering the contributions

to second-order dispersion one gets a value of $\beta_2 \approx 60 \text{ fs}^2/\text{m}$, which gives $L_d \approx 105$ m. These values give $L_{\text{opt}} \approx 1.7$ m, which turns out to be longer than the fiber length used in the experiment. Therefore the effect of dispersion is almost negligible as in the case of argon. A typical broadened spectrum measured using a 20-fs input pulse for a krypton pressure $p = 2.1$ bar and an input peak power $P_0 = 2$ GW is shown in Fig. 4b. In this case one obtains $L_{\text{nl}} \approx 1.1$ cm (for a capillary radius of 80 μm) and $L_d \approx 2$ m ($\beta_2 \approx 60 \text{ fs}^2/\text{m}$), so that the optimum length turns out to be $L_{\text{opt}} \approx 36$ cm, which is close to that used in the experiments (60 cm). Figure 5 shows the results of computer simulations of 20-fs pulse propagation along the hollow fiber in the experimental conditions described above. To obtain a qualitative agreement with the measured spectral broadening we have assumed a nonlinear index coefficient n_2 three times smaller than the quoted value. We can attribute the difference to the uncertainty of the quoted n_2 value, especially for femtosecond pulses. The calculated spectral broadening shows a behavior which is quite close to that observed experimentally. Figure 5b depicts the temporal intensity profile of the pulse at the output of the fiber. The nearly flat-top shape indicates [15] that the use of 20-fs seed pulses can lead to nearly ideal conditions for the generation of linearly chirped pulses in the krypton-filled waveguide.

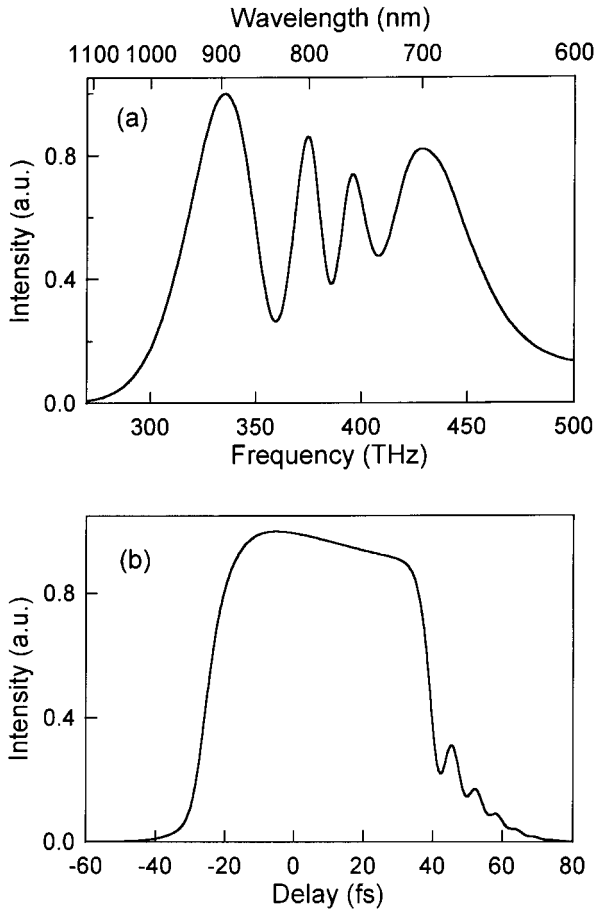


Fig. 5. **a** Spectral broadening obtained by computer simulations of the pulses at the output of a hollow fiber filled with krypton under the same experimental conditions reported in Fig. 4b using 20-fs input pulses. **b** Intensity profile of the pulse at the output of the fiber

2.2.3 Nitrogen. A typical shape of the output spectrum obtained by launching the 140-fs pulses into the fiber at $p = 3$ bar nitrogen pressure and at an input peak power $P_0 = 3.5$ GW is shown in Fig. 6a. The spectrum features deep amplitude modulations typical of a pure SPM process and a clear red shift, which is the signature of a noninstantaneous Kerr response of the medium. In fact in molecular gases both the response from bound electrons and nuclei have to be taken into account. The noninstantaneous contribution to the Kerr response arises from reorientation of the molecules due to their interaction with the optical pulse electric field through the anisotropy of the molecular polarizability [22, 23]. To evaluate the characteristic response time of the nonlinearity we have calculated the spectrum of the pulse after the propagation along the fiber. The measured spectrum is qualitatively reproduced, as shown by the dashed line in Fig. 6a, considering a nonlinearity with a response time of ~ 240 fs. A different situation is observed using 20-fs input pulses. A typical output spectrum at $p = 4$ bar gas pressure and an input peak power of 2.65 GW is shown in Fig. 6b. The broadened spectrum is less deeply modulated and the cut off in the blue side is much less evident. With very short optical pulses the instantaneous electronic contribution to the nonlinear index dominates.

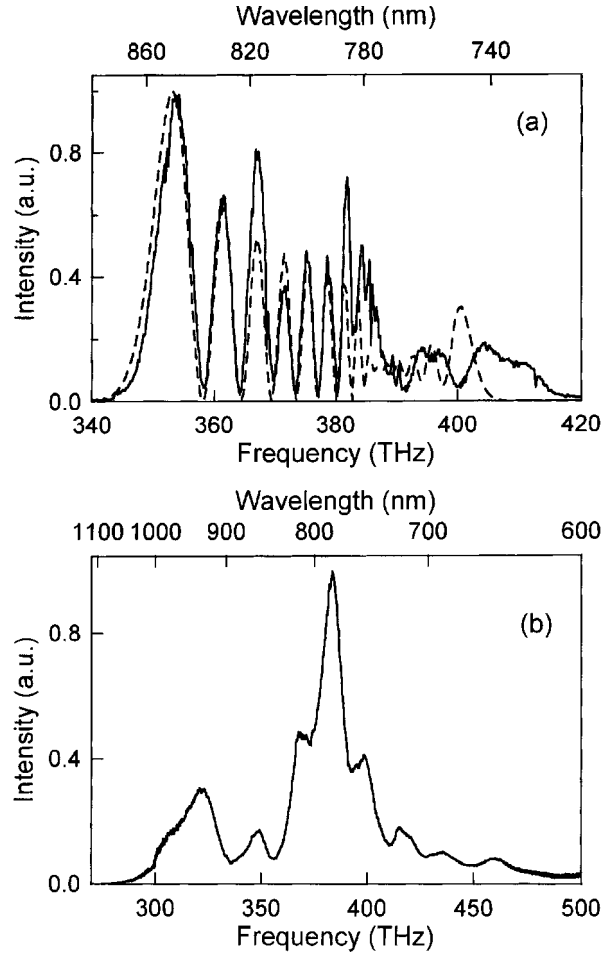


Fig. 6. **a** Spectral broadening (*solid line*) obtained by launching 140-fs pulses into a fiber filled with nitrogen at $p = 3$ bar gas pressure and for an input peak power $P_0 = 3.5$ GW. The *dashed line* shows a calculated spectrum after propagation along the fiber considering a nonlinearity with a response time of ~ 240 fs. **b** Spectral broadening obtained using 20 fs pulses at $p = 4$ bar gas pressure and input peak power of 2.65 GW

3 Pulse compression

Pulse compression experiments with gas-filled hollow fibers were first performed with 140 fs-input pulses. Transform-limited 18-fs and 10-fs pulses were generated respectively, with energies up to 240 μ J [12]. In the following we will report in detail on pulse compression experiments performed using 20-fs input pulses. A broadband high-throughput prism-chirped-mirror dispersive delay line and a specifically designed, low-dispersion interferometric autocorrelator are described in Sect. 3.1 and Sect. 3.2 respectively. The experimental results are reported in Sect. 3.3.

3.1 Prism-chirped mirror dispersive delay line

The frequency-broadened pulses emerging from the hollow fiber were collimated by a silver-coated spherical mirror and propagated through a dispersive delay line which introduced an appropriate group delay $T_g = d\Phi/d\omega$ ($\Phi(\omega)$ is the phase retardation) as shown in Fig. 2. In order that the frequency-broadened pulses can be compressed to their transform limit,

T_g must be precisely controlled over a bandwidth exceeding 130 THz. The ideal T_g variation of the compressor for optimum pulse shortening is depicted in Fig. 7 (*dotted line*). This curve was obtained by taking the opposite of the group delay of the pulse emerging from the output of the hollow fiber (filled with krypton), as inferred from computer simulations. Over the wavelength range of 650–950 nm, this curve notably deviates from a linear behavior due mainly to cubic dispersion in the nonlinear medium. In an attempt to realise the ideal T_g by utilizing wavelength-dependent refraction, a delay line consisting of two pairs of fused silica prisms of small apex angle (20°) was constructed. By using thin wedges instead of the traditionally employed large-angle Brewster-prisms, a substantial reduction of the positive material group delay dispersion (GDD) in the system is allowed for. As a result, less negative GDD is required and high-order phase errors (mainly cubic dispersion) of the prisms can be reduced in proportion to the reduced negative GDD. The variation of T_g with the frequency of the entire system between the output of the fiber and the BBO crystal in the autocorrelator (prism separation 2 m, total propagation in fused silica 15 mm, total propagation length in air 6 m) is shown as a dashed line in Fig. 7. In spite of this improvement, the prismatic system on its own can realize the required T_g only over a bandwidth of ≈ 50 THz because of the excessive negative cubic and quartic dispersion. This bandwidth can be substantially extended with the use of chirped multilayer mirrors (M3 and M4 in Fig. 2), specifically designed to introduce negative GDD in combination with positive cubic and quartic dispersion. The calculated group-delay versus frequency curve (full line in Fig. 7) fits the required delay variation well over a bandwidth of 120 THz for a prism separation set at 1.8 m. The dispersive delay line has a high throughput ($> 85\%$) over the wavelength range of 630–1030 nm. The combination of low loss and appropriate dispersion control over a relative bandwidth $\Delta\omega/\omega_0 > 0.3$ offers the potential for bandwidth-limited single-cycle optical pulse generation.

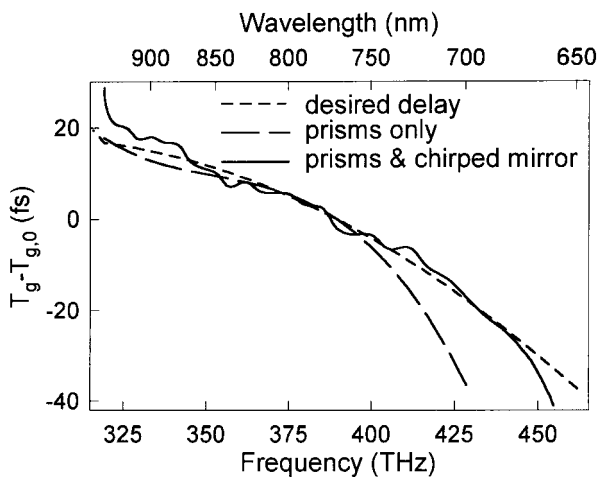


Fig. 7. The desired T_g variation of the compressor for optimum pulse shortening (*dotted line*) as a function of frequency; T_g variation (*dashed line*) obtained using two pairs of prisms; T_g variation (*full line*) using a combination of two pairs of fused silica prisms of 20° apex angle and two chirped multilayer mirrors specifically designed to introduce negative GDD in combination with positive cubic and quartic dispersion

3.2 Interferometric autocorrelator

The compressed pulses were measured by interferometric second harmonic autocorrelation. The uncoated surface of a thin fused silica plate reflects $\approx 10\%$ of the pulse energy into a specifically designed interferometric autocorrelator. To minimize distortions to the ultrashort wavepackets, all reflective optics in the autocorrelator as well as the steering optics in the entire system use silver mirrors protected with low-dispersion dielectric layers. As they enter the autocorrelator the vertically polarized pulses are split, delayed and then recombined by single quarterwave layers of TiO_2 on opposite sides of a 1 mm-thick fused silica substrate (Fig. 2). This ensures a nearly constant 50/50 splitting ratio and negligible dispersion over the entire spectrum of the pulse. This configuration minimizes the overall optical path length in the beam-splitter substrate [24]. Even more importantly, the inherent asymmetry of the conventional geometries with one coating performing both splitting and recombination is eliminated [25]. The asymmetry implies different carrier shifts (with respect to the envelope) in the two replicas of the pulse. This results in an asymmetric second-order interferometric correlation function, severely affecting the evaluation of the pulse width in the few cycle regime. The symmetric configuration shown in Fig. 2 removes this shortcoming. The second-order interferometric autocorrelation signal is generated in a 15- μm -thick BBO frequency-doubling crystal. The time delay in the autocorrelator was calibrated using an He–Ne laser.

3.3 Experimental results

Figure 8a shows the measured second-harmonic interferometric autocorrelation trace obtained with argon when the separation between the two pairs of prisms was set at 2 m. To evaluate the pulse duration, we took the inverse Fourier transform of the spectrum of Fig. 3b and assumed, as a free parameter, some residual cubic-phase distortion, ($d^3\phi/d\omega^3$). A good fit to the experimental data was then obtained with a pulse duration (FWHM) of 5.3 fs and $|d^3\phi/d\omega^3| = 20 \text{ fs}^3$. The precision of this evaluation is mainly affected by possible errors in the measured spectral shape (the spectrograph was calibrated with a standard tungsten lamp) and in the assumed spectral phase; we expect to introduce errors of less than $\pm 10\%$. The minimum pulse duration, as calculated assuming optimum phase distortion compensation, was 5.2 fs. Therefore the pulses can be considered to be almost transform limited. The results of Fig. 8a relate to the case where output pulse energy from the compressor was 40 μJ , corresponding to an input energy to the fiber of 80 μJ . By increasing the input pulse energy to 140 μJ and retaining the same argon pressure, pulses with the same duration with energies up to 70 μJ could be generated. In this case, however, somewhat more pronounced wings appeared in the autocorrelation trace. Figure 8b shows the measured second-harmonic interferometric autocorrelation trace obtained with krypton. From this trace, a pulse duration of 4.5 fs (FWHM) was evaluated with the previously described method, assuming a residual cubic phase distortion $|d^3\phi/d\omega^3| = 10 \text{ fs}^3$. Pulse energy after compression was 20 μJ . These pulses represent the shortest generated to date at the tens of microjoule energy level. The

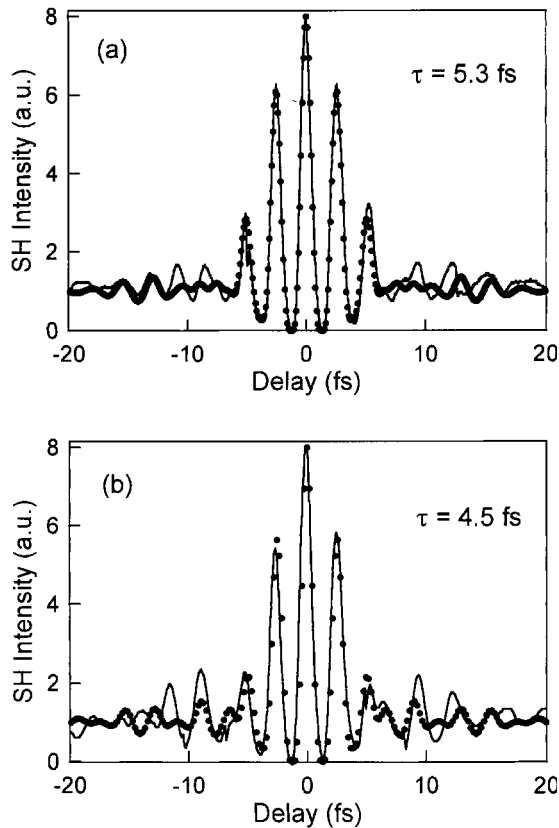


Fig. 8a,b. Measured (solid line) and calculated (dots) interferometric autocorrelation trace of the compressed pulses obtained respectively with (a) argon and (b) krypton using 20-fs input pulses; an evaluation of the pulse duration (FWHM) is also given

minimum pulse duration, estimated from the spectrum shown in Fig. 4b was 4.3 fs; therefore the pulses are almost transform limited. On increasing the input energy to 80 μJ and decreasing the pressure to 1.1 bar in order to maintain constant L_{nl} , slightly longer pulses (5.3 fs) with twice as much energy (40 μJ) were obtained. In the case of nitrogen, by best compression of the pulses whose spectrum is shown in Fig. 6b, a pulse duration of ~ 7 fs was measured. In this case the interferometric autocorrelation exhibited larger wings than in the case of argon and krypton.

4 Output beam characteristics

The polarization state and the spatial coherence of the beam is of crucial importance when it comes to applications of the compressed pulses to nonlinear optical experiments. The beam exiting the waveguide was found to be linearly polarized in the same way as the input beam. The spatial coherence of the beam was investigated by measuring the transverse profile at different distances from the tip of the fiber using a CCD matrix detector without any optical systems in between, in order to avoid aberration effects due to the large spectral bandwidth of the pulses. The measured beam profiles were compared with the calculated intensity profiles assuming free-space propagation of a beam with an initial shape equal to that of the EH_{11} mode of the fiber. The full width at half maximum of the measured beam profiles is plotted in

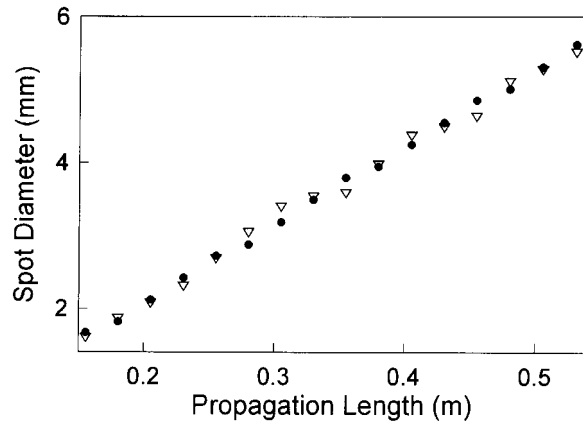


Fig. 9. Measured full width at half maximum of the output beam profile (triangle) as a function of the distance from the tip of fiber; calculated values (dots) from free space propagation of a beam with an initial profile equal to the EH_{11} mode of the fiber

Fig. 9 as a function of the distance from the fiber tip together with the calculated values. The good agreement between the experimental and theoretical results demonstrates that the output beam is diffraction limited. This performance is expected even if the spatial coherence of the input beam is impaired, because the hollow waveguide acts as a distributed spatial filter, suppressing high-frequency spatial components possibly present in the input beam.

5 Prospectives and applications

The potential scalability of this system up to higher pulse energies is an important issue considering the current availability of 20 fs laser pulses with peak powers up to the terawatt level or more. Two considerations play the most important role.

Firstly, the laser peak power must be smaller than the critical power P_c for self-focusing (for a Gaussian beam $P_c = \lambda^2/2\pi n_2$). This sets a constraint on the type of noble gas used and its pressure. Secondly, the laser peak intensity should not exceed the multiphoton ionization threshold which applies for the given pulse duration. This represents a constraint to the hollow fiber diameter and to the type of gas used. By a combination of gas type and proper choice of fiber diameter, and since the threshold for multiphoton ionization increases with decreasing pulse duration [26, 27], the hollow-fiber technique may be scaled up to pulse energies of a few millijoules using input pulses of ~ 20 fs duration.

The generation of diffraction-limited multigigawatt light transients in the single-cycle regime promises to be a powerful tool for precisely triggering and controlling the evolution of atomic systems in strong laser fields. Many applications will benefit from this capability in the future. Perhaps one of the most challenging is the generation and control of high-order harmonic radiation in the soft X-ray spectral region. Coherent X-rays [28] are significant for a number of fields in science and technology because of their potential for providing high spatial and temporal resolution. The accumulation of ionization from the atomic ensemble during exposure to many optical cycles of currently available intense femtosecond pulses tends to gradually decrease the number of neutral

atoms as the light intensity evolves to its peak value. With decreasing pulse duration, however, the fractional number of atoms ionized by the leading edge of the pulse decreases, allowing higher peak laser intensities to be used and thus higher photon energies to be generated. In fact the shortest harmonic wavelengths generated to date (≈ 6 nm) have been produced using the shortest available pulses (≈ 25 fs) with sufficient energy [29]. It has been predicted in a number of theoretical papers [30–32] that the strongly driven atoms emit soft X-rays as a train of short pulses separated by half an optical cycle. Individual pulses in the train have a duration of 100 as. Driving the atomic system with quasi-single-cycle pulses would also allow the production of single-attosecond pulses with a much higher efficiency.

Acknowledgements. We wish to thank R. Szipöcs and K. Ferencz from the Research Institute for Solid State Physics Budapest for the design and manufacturing of the chirped mirrors and L. Pallaro for valuable technical support. This research was supported by the CNR and the Istituto Nazionale per la Fisica della Materia in Italy and by the FWF and the Ministry of Science and Arts in Austria under grants P9710 and P11109.

References

1. P.M.W. French: Rep. Prog. Phys. **58**, 169 (1995)
2. R. Szipöcs, K. Ferencz, Ch. Spielmann, F. Krausz: Opt. Lett. **19**, 201 (1994)
3. L. Xu, Ch. Spielmann, F. Krausz, R. Szipöcs: Opt. Lett. **21**, 1259 (1996)
4. I.D. Jung, F.X. Kärtner, N. Matuschek, D.H. Sutter, F. Morier-Genoud, G. Zhang, U. Keller, V. Scheuer, M. Tilsch, T. Tschudi: Opt. Lett. in press (1997)
5. M. Lenzner, Ch. Spielmann, E. Wintner, F. Krausz, A.J. Schmidt: Opt. Lett. **20**, 1397 (1995)
6. S. Backus, J. Peatross, C.P. Huang, M.M. Murnane, H.C. Kapteyn: Opt. Lett. **20**, 2000 (1995)
7. J. Zhou, C.P. Huang, M.M. Murnane, H.C. Kapteyn: Opt. Lett. **20**, 64 (1995)
8. C.P.J. Barty, T. Guo, C. Le Blanc, F. Raksi, C.R.-P. Petruck, J. Squier, K.R. Wilson, V.V. Yakovlev, K. Yamakawa: Opt. Lett. **21**, 668 (1996)
9. J.P. Chambaret, C. Le Blanc, G. Chériaux, P. Curley, G. Darpentigny, P. Rousseau, G. Hamoniaux, A. Antonetti, F. Salin: Opt. Lett. **21**, 1921 (1996)
10. R.L. Fork, C.H. Brito Cruz, P.C. Becker, C.V. Shank: Opt. Lett. **12**, 483 (1987)
11. A. Baltuska, Z. Wei, M.S. Pshenichnikov, D.A. Wiersma: Opt. Lett. **22**, 102 (1997)
12. M. Nisoli, S. De Silvestri, O. Svelto: Appl. Phys. Lett. **68**, 2793 (1996)
13. M. Nisoli, S. De Silvestri, O. Svelto, R. Szipöcs, K. Ferencz, Ch. Spielmann, S. Sartania, F. Krausz: Opt. Lett. **22**, 522 (1997)
14. E.A.J. Marcatili, R.A. Schmelzter: Bell. Syst. Tech. J. **43**, 1783 (1964)
15. G.P. Agrawal: Nonlinear Fiber Optics, 2nd. edn. (Academic, San Diego, 1995)
16. W.J. Tomlinson, R.H. Stolen, C.V. Shank: J. Opt. Soc. Am. B **1**, 139 (1984)
17. H.J. Lehmeier, W. Leupacher, A. Penzkofer: Opt. Commun. **56**, 67 (1985)
18. A. Dalgarno, A.E. Kingston: Proc. R. Soc. London, Ser. A **259**, 424 (1966)
19. T.K. Gustafson, J.P. Taran, H.A. Haus, J.R. Lifshitz, P.L. Kelley: Phys. Rev. **177**, 306 (1969)
20. R.R. Alfano, S.L. Shapiro: Phys. Rev. Lett. **24**, 1217 (1970)
21. W.H. Knox, R.L. Fork, M.C. Downer, R.H. Stolen, C.V. Shank: Appl. Phys. Letters **46**, 1120 (1985)
22. C.H. Lin, J.P. Heritage, T.K. Gustafson, R.Y. Chiao, J.P. McTague: Phys. Rev. A **13**, 813 (1976)
23. J.F. Ripoche, G. Grillon, B. Prade, M. Franco, E. Nibbering, R. Lange, A. Mysyrowicz: Optics Commun. **135**, 310 (1997)
24. C.P.J. Barty, B.E. Lemoff, C.L. Gordon III: SPIE Proceedings of Generation and Measurement of Ultrashort Pulses Conference, (SPIE Publishing, Bellingham, 1993)
25. Ch. Spielmann, L. Xu, F. Krausz: Appl. Opt. (to be published)
26. J. Zhou, J. Peatross, M.M. Murnane, H.C. Kapteyn, I.P. Christov: Phys. Rev. Lett. **76**, 752 (1996)
27. I.P. Christov, J. Zhou, J. Peatross, A. Rundquist, M.M. Murnane, H.C. Kapteyn: Phys. Rev. Lett. **77**, 1743 (1996)
28. M.H. Key: Nature **316**, 314 (1985)
29. J. Zhou, J. Peatross, M. Murnane, H.C. Kapteyn: Phys. Rev. Lett. **76**, 752 (1996)
30. P.B. Corkum: Opt. Photon. News **6**, 18 (1995)
31. M. Ivanov, P.B. Corkum, T. Zuo, A. Bandrauk: Phys. Rev. Lett. **74**, 2933 (1995)
32. P. Antoine, A. L'Huillier, M. Lewenstein: Phys. Rev. Lett. **77**, 1234 (1996)